Memoirs of the Faculty of Engineering, Kyushu University, Vol.66, No.2, June 2006

Experimental Studies on Lateral Blowing for the Improvement of Aerodynamic Characteristics of Reusable Launch Vehicles in Subsonic Flow

by

Kenji TADAKUMA[*], Takuro ISHIDA[**] , Shigeru ASO[***]
and Yasuhiro TANI[†]

(Received May 22, 2006)

Abstract

An experimental study on the improvement of aerodynamic characteristics of RLVs (Reusable Launch Vehicles) due to lateral blowing has been conducted. A square and a triangular cross sections of fuselage have been considered in order to investigate effects of shape of cross section of fuselage on aerodynamic characteristics during lateral blowing. And four different planform wings have been considered to evaluate effects on planform of wing during lateral blowing. Results show that lateral blowing increases lift of the models over a wide range of angle of attack. Especially a significant increase in lift is achieved in the case of a "square" model at high angle of attack. Increase of lift due to lateral blowing is obtained in all wing types over a wide range of angle of attack. The resulting lift of the model with small sweepback angle and a rectangular wing is lager than that of the other wings in high angle of attack region. As a result of calculation of landing process, lateral blowing makes possible a shorter landing distance or a smaller landing velocity of a RLV.

Keywords: Lateral blowing, Lift augmentation, Subsonic flow, Fuselage cross section, Square, Triangular, Sweepback angle, Landing

Nomenclature

C_D	=	drag coefficient
C_L	=	lift coefficient
C_{my}	=	pitching moment coefficient
C_{Fj}	=	jet-reaction-force coefficient ($=2F_j/(qS_{ref})$)

[*] Graduate Student, Department of Aeronautics and Astronautics
[**] Undergraduate Student, Department of Aeronautics and Astronautics
[***] Professor, Department of Aeronautics and Astronautics
[†] Assistant Professor, Department of Aeronautics and Astronautics

C_μ = jet momentum coefficient (= $\dot{m}_j V_j/(qS_{ref})$)
F_j = jet reaction force (one-side jet)
F_{njt} = aerodynamic force without main flow, with jet and tubes
F_{wjt} = aerodynamic force with main flow, jet and tubes
F_{wnn} = aerodynamic force with main flow, without jet and tubes
F_{wnt} = aerodynamic force with main flow, without jet and with tubes
L_m = full length of models
L/D = lift-to-drag ratio
$\dot{m}_j V_j$ = jet mass flow rate
M_∞ = free-stream Mach number
p_{aj} = atmosphere pressure
p_{ej} = jet-exit pressure
p_0 = stagnation pressure at adjacent to nozzle-exit before blowing
p_{0j} = stagnation pressure of a small tank attached on the way of tubes to the model
q = dynamic pressure
Re = Reynolds number (=$U_\infty L_m/\nu$)
S_j = area of nozzle exit
S_{ref} = projection area of model
U_∞ = free-stream velocity
V_j = jet velocity
α = angle of attack
γ = specific heat ratio
σ^* = critical flow coefficient (=$[\gamma\{2/(\gamma+1)\}^{(\gamma+1)/(\gamma-1)}]^{1/2}$)

1. Introduction

Space transportation system is one of the most important infrastructures for space activities. Low cost, improvement of reliability and safety are important subjects for the development of RLV (Reusable Launch Vehicle).

One of the most important problems is to achieve high aerodynamic performance. High lift performance at low speed regime makes possible a shorter landing distance. High lift-to-drag ratio performance allows easy approach during landing process and larger down and cross range in high speed region.

The RLVs are mostly classified into two types, wing-body type vehicles (e.g. Space Shuttle) and lifting-body type vehicles (e.g. X-33). The wing-body-type vehicles have good aerodynamic performance in subsonic and transonic regions. However the vehicles have higher aerodynamic heating than the lifting-body type due to small radius of the leading edges. Although increase of the leading-edge radius can reduce the aerodynamic heating, the vehicles can not avoid the aerodynamic heating at stagnation points of the leading edges and significant local aerodynamic heating due to shock-shock interactions[1]. Therefore small wings with reduced area affected by aerodynamic heating and weight are advantageous to RLV. However decrease in lift would result from small wings. Such a RLV needs to increase the lift generated from the fuselage than the previous one. At subsonic speeds, Sigal et al have shown that the cross sectional shapes of slender bodies have significant effects on aerodynamic characteristics[2,3]. Morita et al have reported the aerodynamic characteristics of RLVs with triangle and rectangular fuselage-cross sections[4]. According to the reports, in subsonic region, a triangular model is superior to a square model on the aerodynamic performance. However a vehicle with a triangular-fuselage-cross

section is undesirable from a vehicle design point of view (e.g., volume, engine mount). To remove some of the disadvantages, it is important to increase aerodynamic performance for configurations with a larger volume. In addition, enhancement of the aerodynamic performance for vehicles with triangular-fuselage-cross section can also provide benefits in the presence of the design limitations.

Therefore we apply lateral blowing to the RLVs with various types of fuselage-cross sections in order to achieve improved aerodynamic performance. Lateral blowing is realized by injecting a pair of sonic jets parallel to the trailing edge of the wing. In the past, several experimental studies and computations on the subject of lateral blowing have been conducted[5-9]. They have reported improvement of aerodynamic characteristics of the low aspect wing and shed light as to the mechanism of the lift increase. Figure 1 shows a schematic view of the flow field in a lateral blowing[8]. At first, lateral blowing increases negative pressures on the upper surface of the wing due to the accelerated flow by the jet. Secondly the jet stream works as an obstacle lying laterally normal to the main flow. Therefore the pressure on the wing lower surface increases. In addition, Karashima and Tadakuma have reported that lateral blowing increased the strength of leading-edge separation vortex at high angle of attack[5,10]. In other words, lateral blowing improves aerodynamic characteristics regardless whether a leading-edge separation vortex exists or not. Therefore lateral blowing increases the lift over a wide range of angle of attack as compared to other blowing techniques which directly control leading-edge separation vortices[11-16]. However, experimental studies of RLVs on the effects of the fuselage-cross section in lateral blowing have not been conducted. In the present study, we examine two types of triangular and rectangular cross-sectional bodies with wings.

In addition, it is important for applying the lateral blowing to actual vehicles to investigate aerodynamic effects on planforms of wing due to lateral blowing. However studies on the effects in lateral blowing have not been conducted.

Objective of the present study is to investigate effects and the mechanism during lateral blowing on different fuselage configurations and various platforms of wing in the improvement of aerodynamic performance for RLV. RLVs of wing-body type have delta wings for supersonic flight. However delta wings don't have good aerodynamic performances at low speed regime. Vehicles for space transportation system should have satisfactory aerodynamic performance at low speed for safe approach and landing. In this paper, we report experimental results at M_∞=0.29 and U_∞=20 m/s illustrating the improvement of low-speed aerodynamic characteristics due to lateral blowing, and the result of possible application for landing process.

2. Experimental Apparatus and Procedures

2.1 Wind tunnel

Tests have been conducted in a blow-down type wind tunnel of ISAS, JAXA with 600 mm×600 mm square test section and a circuit wind tunnel of Kyushu University with 2000 mm×2000 mm circular test section

2.2 Model and experimental apparatus

Figure 2 and **Figure 3** show the schematic view and photograph of the models to investigate effects on different fuselage cross sections. The "Triangular" model means the wing-body model with triangular-fuselage-cross section and "Square" model means the wing-body model with a square-fuselage-cross section. The main wings and the projected fuselage have the same area equal to 0.0314 m^2, a reference area in the present study. As shown in **Fig.3**, the fuselage cross

section smoothly varies from a triangle or a square to a circle toward the nose. The nose tip of these models has the same radius of 7 mm. And each corner of the “square” and “triangular” cross sections has the same radius of 6 mm. The wings of these models have a delta planform of modified NACA0010 with 45° sweepback. The wing cross section of the vertical tail is NACA0006 with sweepback angles of 45° and 66.5° for the leading and trailing edges respectively. The full length is 0.3448m and used as a reference length. Center of the balance is located at 231 mm behind the nose of the model and the location is used for reference moment center.

Figure 4 shows the schematic view of the models to investigate effects on different planforms of wing. Four wings have been considered: flat delta wing with 72.7° sweepback angle, flat double delta wing with 72.7°/52.2° sweepback angle, flat delta wing with 52.2° sweepback angle and a rectangular wing with NACA0012 cross section.

Devices for the lateral blowing are installed at the bottom of the fuselage providing a lateral jet along the trailing edge of the wing root. Diameter of the jet exit nozzle is 2 mm. Direction of the blowing is perpendicular to the body axis and parallel to the trailing edge of the wing. Devices for the blowing are retracted into the fuselage for no-blowing condition in order to remove parasite drag and aerodynamic heating at the devices.

Figure 5 and **Figure 6** show schematic diagrams of the experimental apparatus. Lateral blowing is realized by injecting a pair of sonic jets in parallel to the trailing edge of the wing. An air compressor as the source of the jet supply is located outside the wind tunnel. Compressed air is loaded to the connector behind the model through a tube. In **Fig. 5**, experiment to investigate effects of fuselage cross section, lift, drag and moment are measured by a sting-type internal balance located into the models. In **Fig. 6**, experiment to investigate effects of planform of wing, lift, drag and moment are measured by a 3-component balance located on the root of the strut.

2.3 Methodology to determine jet momentum

It is general for determining jet momentum to measure stagnation pressure at adjacent to jet exit before blowing (=p_0) during the experiment where we measure the aerodynamic force, and use the equation for isentropic flow. However, it is difficult to measure the stagnation pressure p_0 during the experiment because of the laboratory equipment. Therefore, in the present study, stagnation pressure of a small tank attached on the way of tubes to the model (=p_{0j}) during the aerodynamic experiment was measured. It is necessary for estimating the jet momentum to calculate the stagnation pressure p_0 by using the small-tank stagnation pressure p_{0j} in any methodology because relation of the small-tank stagnation pressure p_{0j} and the stagnation pressure p_0 at adjacent to the nozzle exit before blowing is not isentropic due to existence of corners and contracted flow in flow channel for blowing. Therefore, in the present study, we measured some jet reaction force F_j with some small-tank stagnation pressure p_{0j} in the early experiment in a constant atmosphere pressure p_{aj}. The stagnation pressure p_0 can be estimated by using the measured jet reaction force F_j, the atmosphere pressure p_{aj} and Eq. (1c). Eq. (1a) means jet reaction force which is sum of momentum and pressure thrust. Eq. (1b) is given by relation of isentropic flow for convergent nozzle. Eq. (1c) is determined by Eq. (1a) and Eq. (1b). **Figure 7** shows a schematic view of the early experiment that measures the jet reaction force F_j. **Figure 8** shows the relation of the small-tank stagnation pressure p_{0j} and the stagnation pressure p_0 near the nozzle exit before blowing. Accordingly we can obtain the jet momentum by using the determined small-tank stagnation pressure p_{0j} and Eq. (2). The coefficient 1/2 in front of the jet momentum expresses one-side jet.

$$F_j = 1/2\dot{m}_j V_j + \left(p_{ej} - p_{aj}\right)S_j \tag{1a}$$

Where, $1/2\dot{m}_j V_j = \left[2\gamma/(\gamma+1)\right]^{1/2} S_j \sigma^* p_0$, $p_{ej}/p_0 = \left[2/(\gamma+1)\right]^{\gamma/(\gamma-1)}$ (1b)

Therefore, $F_j = p_0 S_j \left\{\sigma^* \left[2\gamma/(\gamma+1)\right]^{1/2} + \left[2/(\gamma+1)\right]^{\gamma/(\gamma-1)}\right\} - p_{aj} S_j$ (1c)

$$1/2\dot{m}_j V_j = \left[2\gamma/(\gamma+1)\right]^{1/2} S_j \sigma^* p_0 \quad (2)$$

2.4 Test conditions

Test conditions are shown in **Table 1** and **Table 2**. Aerodynamic characteristics on the lift, drag and pitching moment are measured. Oil flow technique was used for flow visualization. It is generally used a jet momentum coefficient C_μ to evaluate the effect of blowing which is defined in Eq. (3).

$$C_\mu = \dot{m}_j V_j / \left(qS_{ref}\right) \quad (3)$$

2.5 Evaluation method of aerodynamic forces due to lateral blowing

Aerodynamic forces measured in the balance during the blowing include the influence due to the internal pressure of the tubes because compressed air for the blowing is supplied from the tubes attached at the back of the model. In addition, aerodynamic forces during the blowing include those of the tubes. Therefore we need to remove these influences when we evaluate the blowing effect on the overall aerodynamic characteristics. Accordingly aerodynamic forces due to blowing (=δF) are obtained by Eq. (4). The quantity "F_{wjt}-F_{njt}" refers to the difference between forces during a blowing condition at M_∞=0.29 ("wind-on" condition) and at M_∞=0 ("wind-off" condition). The quantity "F_{wnt}-F_{wnn}" refers to the difference between forces for the with-tube condition and no-tube condition at M_∞=0.29 ("wind-on" condition). In the present study, correction on the base pressure has not been applied.

$$\delta F = F_{wjt} - F_{njt} - \left(F_{wnt} - F_{wnn}\right) \quad (4)$$

2.6 Measurement uncertainties

Uncertainties in the measured data estimated using the methodology of AIAA Standard and other reference[17,18]. Those uncertainties (two-sided 95% confidence interval) are shown figures as error bars.

3. Results and Discussions

3.1 Effect of fuselage cross section

3.1.1 Aerodynamic characteristics

Figure 7 and **Figure 8** show the results of aerodynamic coefficients of the "Triangular" and "Square" models at M_∞=0.29. In the figure, "Lateral Blowing of C_μ=0.015" refers to aerodynamic characteristics corresponding to a lateral blowing of C_μ=0.015. "Model only" refers to the case of the wing-body model without the devices for blowing. "Model + Lateral blowing devices" refers to the model including the devices for blowing. **Figure 9(a)** shows that with lateral blowing case is achieved increase of C_L over a wide range of angle of attack and at constant increments of C_L until 12.5° of angle of attack. In addition, larger increase of C_L is obtained above 15°. Increase of C_L reaches a maximum around 20°-25° angle of attack. The resulting C_L is almost 10% larger than that of the "Model + Lateral Blowing Devices". **Figure 9(b)** shows the

results of drag coefficient C_D which increases with the angle of attack in the lateral blowing condition. The drag polar curves are shown in **Fig. 9(c)**. Lateral blowing improve C_L-C_D characteristics as compared to those of the "Model + Lateral Blowing Devices" and "Model only" in high angle of attack region. Pitching moment coefficients are shown in **Fig. 9(d)**. Positive C_{my} indicates a nose-up moment. The moment reference center is located at 231 mm behind the nose. In this figure, it can be seen that the lateral blowing enhances the nose-down pitching moment.

Figure 10 shows aerodynamic characteristics of the "Square" model at M_∞=0.29. Trend on the aerodynamic characteristics due to lateral blowing is almost same as that of the "Triangular" model. However, the increment of the lift increase by the lateral blowing around stall angle is different. From the **Fig. 10(a)**, it can be seen a remarkable lift increase in high angle of attack region as compared to that of the "Triangular" model. The lateral blowing increases the C_{Lmax} and the stall angle of the "Square" model.

3.1.2 Oil flow visualization

Oil flow visualization has been conducted to investigate the mechanism of the lift increase due to lateral blowing. **Figure 11**-**Figure 13** show the oil-flow visualization results at α=25 °, C_μ =0.015 and M_∞=0.29 in the case of the "Triangular" and "Square" model. This case provides a maximum lift increase of the "Square" model. Some lines along the oil flow patterns are illustrated in magnified figures of those oil flow visualization results to give easier viewing.

Figure 11 shows a top view of oil flow visualization results. From **Fig. 11(a)**, surface flow of the wing formed streamlines from upper part of the fuselage to tip. These patterns mean separation vortex generated at fuselage is coupled with leading-edge separation vortex from the wing. However, it could not be seen any difference of the blowing and no-blowing cases in the top view of "Triangular" model.

In no-blowing case of **Fig. 11(b)**, we can see that the oil collects around the center of the wing and we can't recognize the flow to the tip. This oil flow pattern shows a breakdown of the leading-edge separation vortex of the wing. From the results of aerodynamic test, the wing is stalled at this angle of attack. The direction of streamlines on the fuselage and the wing is different. Therefore, unlike in the case of "Triangular" model, the separation vortex from the fuselage and from the wing is not combined. The coupled separation vortices of the "Triangular" model probably work on increasing the stall angle. Compared with the no-blowing and blowing cases, streamlines are quite different. At first, surface flow on the trailing edge of wing near fuselage converges slightly to the fuselage due to lateral blowing. Secondary, in the no-blowing case, we could see that the oil collects around the center of the wing. On the other hand, in the blowing case, it can be seen the flow is channeled from inner to outer, that is, the leading edge vortex is recovered. The recovery results from an increase of favorable pressure gradient on the surface due to the low pressure region generated by the jet. In other words, lateral blowing delays the breakdown of the leading-edge separation vortex from the wing.

Figure 12 shows a side view of the trailing edge around the fuselage backward. In **Fig. 12(a)**, it can not be seen any differences of oil flow patterns of the no-blowing and blowing cases. On the contrary, in the case of "Square" model in **Fig. 12(b)**, streamlines on the fuselage near the trailing edge moves toward the trailing edge of the wing due to lateral blowing, though the flow near the trailing edge in the no-blowing case reverses and separates. This means that circulation of the wing is increased.

Figure 13 shows the lower wing surface near the trailing edge. From both of the bottom views with lateral blowing, it can be seen that the jet stream dams up the main flow near the trailing

edge. Jet stream works as an obstacle lying laterally against the main flow. Therefore pressure on the lower surface near the trailing edge increases. In addition, the favorable pressure gradient on the upper wing surface is weakened by the flow on the lower wing surface which streams around the trailing edge to the upper wing surface in high angle of attack region. Considering the effect which the lateral blowing works as an obstacle against main flow, it is possible that lateral blowing prevents the flow on lower surface which streams around trailing edge to upper wing surface, and the adverse pressure gradient on the upper wing surface is weakened. The effect due to the suppression may contribute the delay of breakdown and recovery of leading-edge-separation vortex from the wing.

Mechanism of the lift increase due to lateral blowing on the basis of oil-flow-pattern observation is summarized as follows: in the case of the "Triangular" model, (a) Pressure near the trailing edge on the lower surface is increased because the jet stream works as an obstacle lying in the lateral direction against the main flow. In the case of the "Square" model, in addition to the mechanism of the "Triangular" model, (b) Breakdown of the leading-edge separation vortex is delayed. (c) Circulation is increased. In the case of the "Square" model, the lift increase due to lateral blowing is larger than that of the "Triangular" model. It is possible that lateral blowing is more effective to delay vortex breakdown and separation with rapid stall phenomenon.

3.1.3 Lift augmentation ratio

One way to judge the lifting efficiency of lateral blowing is by examining the lift augmentation ratio $\delta C_L / C_{Fj}$. The effect of α and fuselage configuration on this parameter is presented in **Fig. 14**. The augmentation ratio was larger than 1 at almost all of angle of attack. Larger augmentation ratio was observed with both models in stall angle region. The largest augmentation ratio of 10 was obtained with "Square" model at stall angle, which means that lateral blowing generates ten times the lift that would be obtained if the jet were vectored downward (perpendicular to the freestream). These data suggest that lateral blowing becomes more effective in producing lift than thrust vectoring to downward, especially with "Square" model in high angle of attack region.

3.2 Lift coefficient of different planform wings

Figure 15 shows the results of aerodynamic coefficients of the models with various planforms of wing at U_∞=20 m/s. In the figure, "No Blowing" refers to the case of the models with the devices for blowing, with tubes and without blowing. "Lateral Blowing of C_μ=0.07" refers to aerodynamic characteristics corresponding to a lateral blowing of C_μ=0.07, which is removed the influence due to the internal pressure of the tubes. However aerodynamic characteristics of both symbols include the effects of sting, tubes and strut. These effects plot as "Effects of Sting, Support and Tubes" in figures.

In **Fig. 15**, at "No Blowing", it can be seen that "Delta wing 1" and "Double delta wing" are stalled since the lift coefficient scope of those models is decreased. "Delta wing 2" starts to stall around 32.5 ° , "NACA0012" is stalled at smaller angle than "Delta wing 2". Larger stall angle of these flat delta wings except for "NACA0012" in high angle of attack region results from leading edge separation vortices, which is typical of delta wing. In **Fig. 15**, at "Lateral Blowing C_μ =0.07", increase of lift due to lateral blowing in all wing types is obtained over a wide range of angle of attack. The resulting lift of flat delta wing with 52.2° sweepback angle and 2-dimensional wing with NACA0012 cross section is lager than that of the other wings in high angle of attack region.

3.3 Possible application of lateral blowing for landing process

Advantages of lateral blowing due to experimental studies are summarized as follows: lift is increased over a wide range of angle of attack. Especially, remarkable increase of lift is obtained at high angle of attack. In addition, the stall angle is increased. Therefore, to take a consideration for application to actual RLV, the good performance due to lateral blowing is increase of C_{Lmax}. The increase of C_{Lmax} results in decrease of landing speed. Increase of the performance due to lateral blowing could bring many advantages such as wide selection of landing runway on abort process and decrease the strength of landing gears. Accordingly, lateral blowing increases margin of safety and decreases the weight of landing gears.

In the present study we estimate the effect of lateral blowing in landing by assuming that the lateral blowing is used at flare phase in landing process.

At first, the operating time is estimated to calculate the required air amount for lateral blowing. The conditions for calculation of the air amount are shown in **Table 3**. The conditions refer specifications of Space Shuttle and experimental results[10]. The calculation is used the methodology of Reymer's reference[19]. The required time in flare phase estimated by using the Reymer's methodology and the required air amount are shown in **Table 4**. The required air amount is calculated by integrating to the required time of mass flow rate, which are shown in Eq. (5).

$$\dot{m}_j V_j = 1/2 \rho V_f^2 S_{ref} C_\mu$$

$$V_j = a_0 \{2/(\gamma+1)\}^{1/2} \tag{5}$$

$$\int_0^{9.1} \dot{m}\ \mathrm{dt} = 1{,}321 \text{ kg}$$

Therefore the source of supply is required to select appropriately to decrease the volume and weight for lateral blowing at application to actual RLV. The sources of supply include jet engine, compressor and pressure container. Jet engine and compressor is better than pressure container as a source of supply in terms of reduction of the weight. However trade-off analysis between its increase of weight and the increase of lift due to lateral blowing is required.

4. Conclusions

Experimental studies are conducted in order to investigate the effect of lateral blowing on the improvement of aerodynamic characteristics of RLVs and also to reveal the flow mechanism of the lateral blowing. The experiments have been conducted under the conditions of M_∞=0.29 and U_∞ =20 m/s. Conclusions of the present study are summarized as follows:

1) The increase of lift is achieved by lateral blowing over a wide range of angle of attack for both "Triangular" and "Square" models. Larger lift increase is observed at high angle of attack. The largest lift increase is obtained in the case of a "Square" model at stall angle. Lateral blowing can be useful to increase C_{Lmax} and stall angle for the "Square" model.
2) The flow Mechanism of the lift increase due to lateral blowing through careful observation of oil-flow-pattern on the models is summarized as follows: in the case of the "Triangular" model, (a) Pressure near the trailing edge on the lower surface is increased because the jet stream works as an obstacle lying in the lateral direction against the main flow. In the case of the "Square" model, in addition to the same mechanism which is also observed in the "Triangular" model, (b) the breakdown of the leading-edge separation vortex is delayed due to lateral blowing. And (c)

the circulation of the wing is increased.

3) Lateral blowing becomes more effective in producing lift than the thrust of the jet vectoring to downward, especially with “Square” model in high angle of attack region.

4) Survey on application of lateral blowing to landing process is conducted. The results show that the trade-off analysis between increase of weight due to source of air supply for lateral blowing and increase of lift due to lateral blowing will be required. However, the high promising capability of lateral blowing is proved through the present survey.

References

1) Zoby, E. V., Thompson, R. A., and Wurster, K. E., ”Aeroheating Design Issues for Reusable Launch Vehicles A Perspective,” AIAA paper 2004-2535, Jun. 2004.

2) Sigal, A., “Aerodynamic characteristics of rectangular cross-sectional bodies at M = 0.85,” Journal of Aircraft, Vol. 25, No. 11, 1988, pp. 1018-1022.

3) Sigal, A., and Lapidot, E., “Aerodynamic Characteristics of Configurations Having Bodies with Square , Rectangular , and Circular Cross Sections,” Journal of Aircraft, Vol. 26, No. 2, 1989, pp. 85-89.

4) Morita, W., Aso, S., and Tani, Y., ” Experimental Study on Effects of Fuselage Configurations for RLV on Aerodynamic Characteristics,” AIAA paper 2004-2151, Jun. 2004.

5) Karashima, K., “Augmentation of Aerodynamic Performance of Low Aspect-Ratio Wings by Use of a Lateral Blowing at the Trailing Edge,” The 28th Fluid Dynamics Conferences, JSASS, Japan, 1996, pp. s-17-s-26.

6) Kamishita, M., and Aso, S., “A Study on Improvement of Aerodynamic Characteristics of the Next-Generation SST Wing by Lateral Blowing in Subsonic Flow,” Journal of The Japan Society for Aeronautical and Space Sciences, Vol. 49, No. 569, 2001, pp. 174-180.

7) Aso, S., Kamishita, M., Karashima, K., and Sato. K., “A Study on Active Flow Control for Next-Generation SST for Higher L/D,” AIAA Paper 2002-2844, Jun. 2002.

8) Kamishita, M., Aso, S., Karashima, K., and Sato. K., “Improvement of Aerodynamic Characteristics of Next-Generation SST Wing by Lateral Blowing,” Proceedings of 22nd International Congress of Aeronautical Sciences, Sep. 2000.

9) Miyaji, K., Fujii, K., and Karashima, K., “Enhancement of the Leading-Edge Separation Vortices by Trailing-Edge Lateral Blowing,” AIAA Journal, Vol. 34, No. 9, 1996, pp. 1943-1945.

10) Tadakuma, K., Aso, S., and Tani, Y., “Active Control of Aerodynamic Characteristics of Space Transportation System by Lateral Blowing,” AIAA Paper 2004-2718, Jun. 2004.

11) Bradley, R. G., and Wray, W. O., “A Conceptual Study of Leading-Edge-Vortex Enhancement by Blowing,” Journal of Aircraft, Vol. 11, No. 1, 1974, pp. 33-38.

12) Hong, J. S., Celik, Z. Z., and Roberts, L., “Effect of Leading-Edge Lateral Blowing on Delta Wing,” AIAA Journal, Vol. 34, No. 12, 1996, pp. 2471-2478.

13) Wong, G. S., Rock, S. M., Wood N. J., and Roberts, L., “Active Control of Wing Rock Using Tangential Leading-Edge Blowing,” Journal of Aircraft, Vol. 31, No. 3, 1994, pp. 659-665.

14) Campbell, F. J., “Augmentation of Vortex Lift by Spanwise Blowing,” Journal of Aircraft, Vol. 13, No. 9, 1976, pp. 727-732.

15) Seginer, A., and Salomon, M., “Performance Augmentation of a 60-Degree Delta Aircraft Configuration by Spanwise Blowing,” Journal of Aircraft, Vol. 23, No. 11, 1986, pp. 801-807.

16) Wood, J., and Roberts, L., “Control of Vortical Lift on Delta Wings by Tangential Leading-Edge Blowing,” Journal of Aircraft, Vol. 25, No. 3, 1988, pp. 236-243.

17) AIAA standard, “Assessment of Experimental Uncertainty with Application to Wind Tunnel Testing,” AIAA S-071A-1999, 1999.
18) Kline, S. J., and McClintock, F. A., “Describing Uncertainties in Single Sample Experiments,” Mechanical Engineering, Vol. 75, No. 1, 1953, pp. 3-8.
19) Reymer, P. D., “Aircraft Design : A Conceptual Design,” AIAA Education Series, 1999, pp. 563-569.

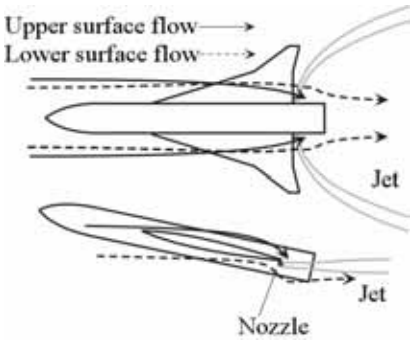

Fig. 1 Schematic flowfield of lateral blowing.[8)]

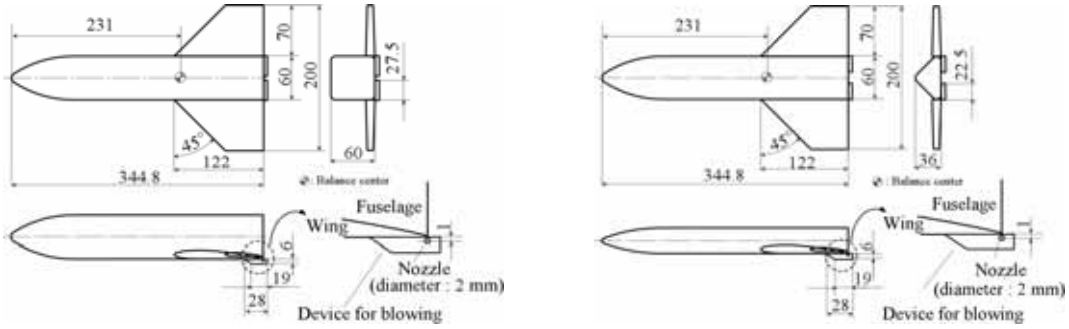

(a) “Square” model (b) “Triangular” model

Fig. 2 Schematic view of the experimental models.

(a) “Square” model (b) “Triangular” model

Fig. 3 Experimental models (photograph).

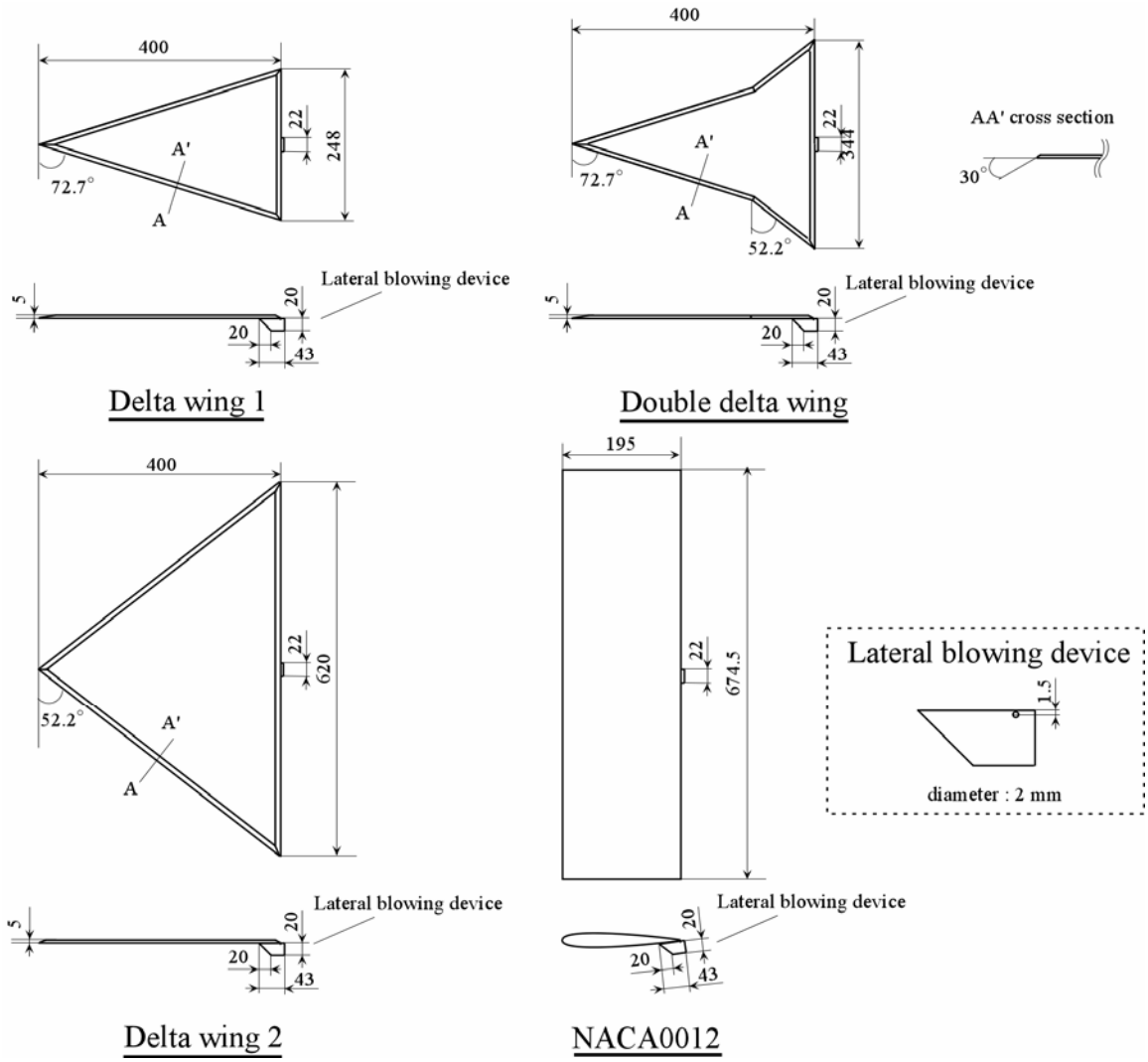

Fig. 4 Schematic view of the experimental models.

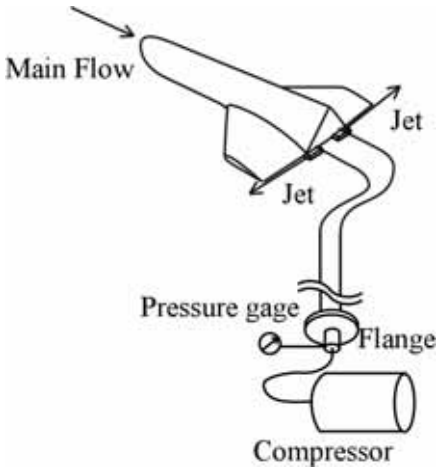

Fig. 5 Experimental apparatus.

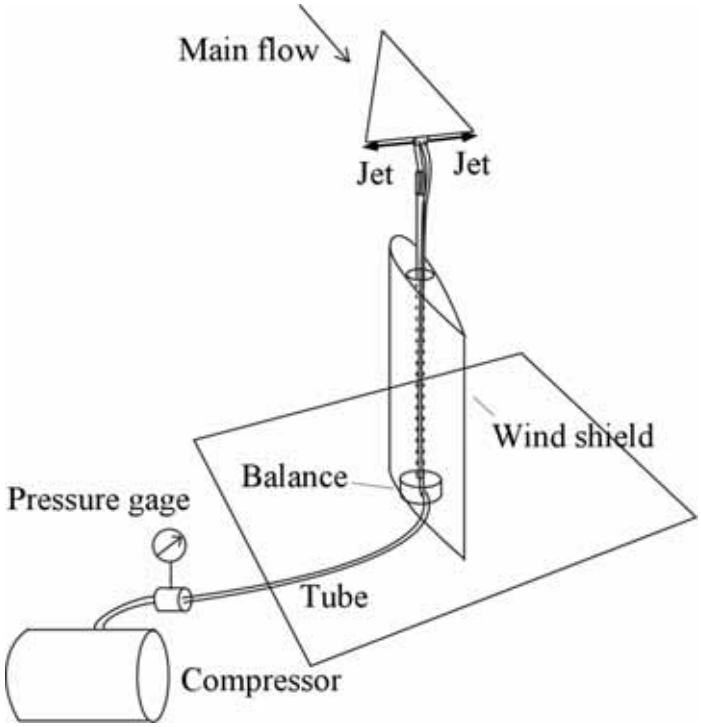

Fig. 6 Experimental apparatus.

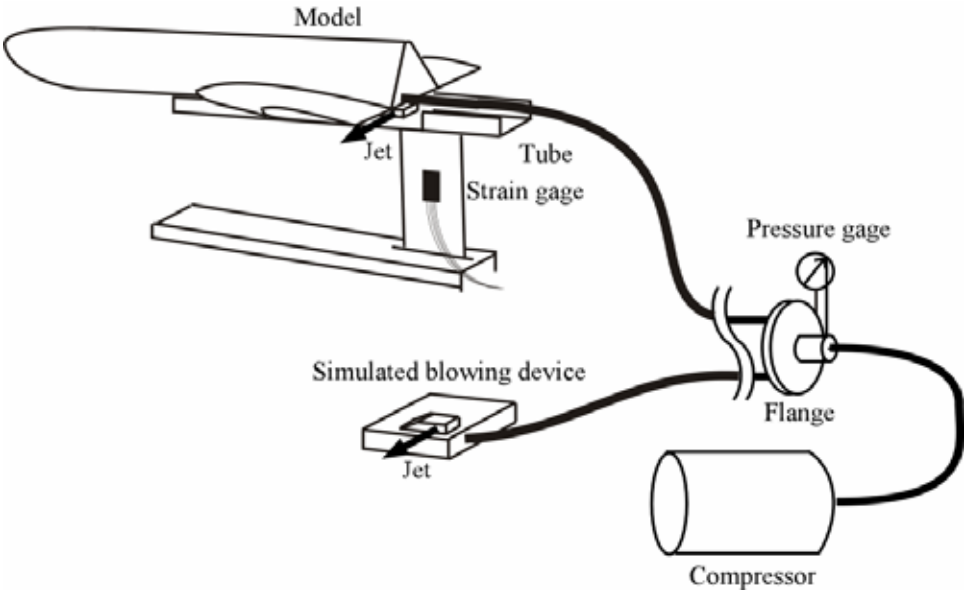

Fig. 7 Earlier experiment to measure the jet reaction force.

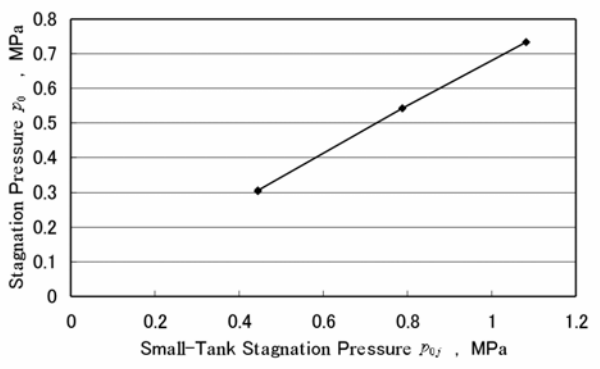

Fig. 8 Relation of the small-tank stagnation pressure p_{0j} and the stagnation pressure p_0.

Table 1 Test conditions for "fuselage cross section" experiments.

M_∞	model	C_μ	R_e
0.29	"Triangular"	0.015	3.1×10^6
0.29	"Square"	0.015	3.1×10^6

Table 2 Test conditions for "planform of wing" experiments.

U_∞ [m/s]	model	C_μ	R_e
20	"Delta wing 1"	0.07	5.3×10^5
20	"Delta wing 2"	0.07	5.3×10^5
20	"Double delta wing"	0.07	5.3×10^5
20	"NACA0012"	0.07	2.6×10^5

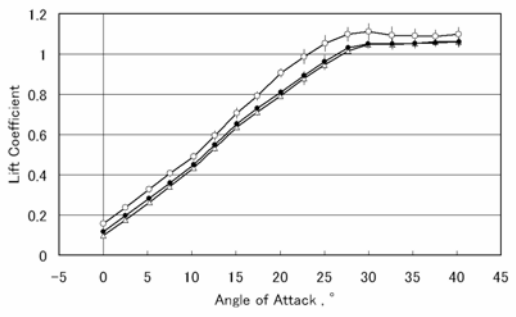

(a) Lift coefficient

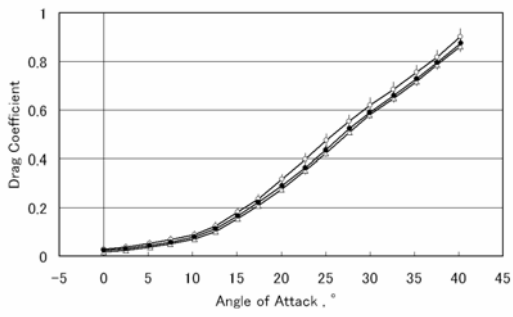

(b) Drag coefficient

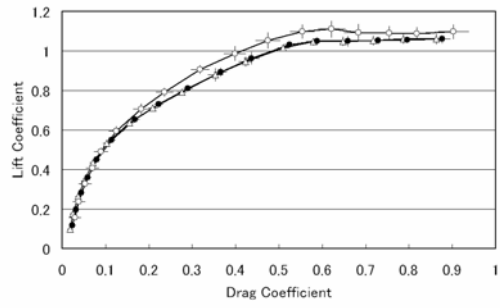

(b) Polar curve

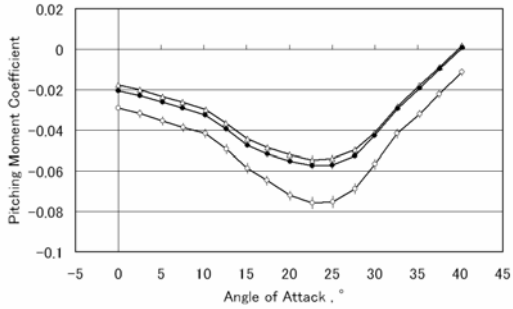

(d) Pitching moment coefficient

Fig. 9 Aerodynamic characteristics of "Triangular" model at M_∞=0.29.

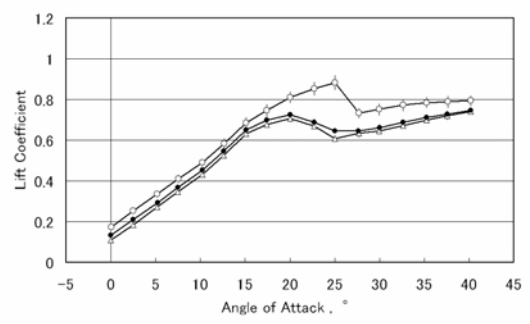

(a) Lift coefficient

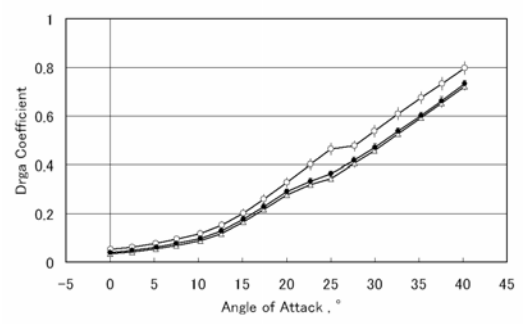

(b) Drag coefficient

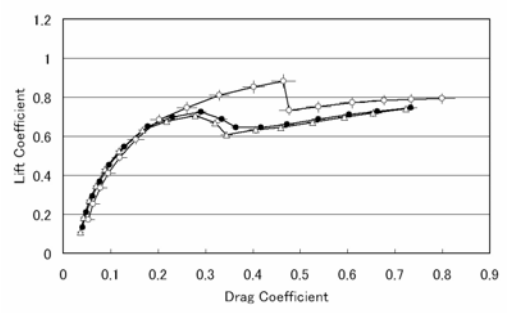

(b) Polar curve

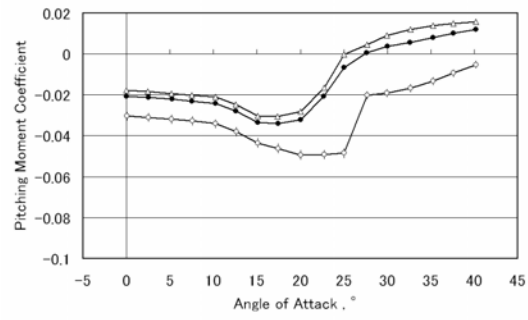

(d) Pitching moment coefficient

Fig. 10 Aerodynamic characteristics of "Square" model at M_{∞}=0.29.

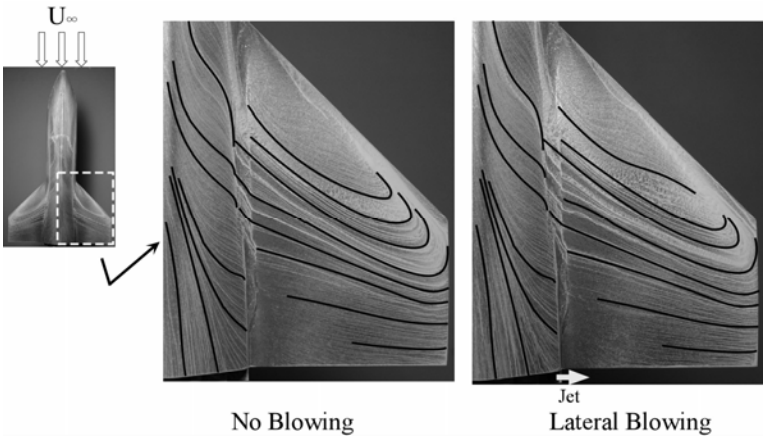

(a) "Triangular" model

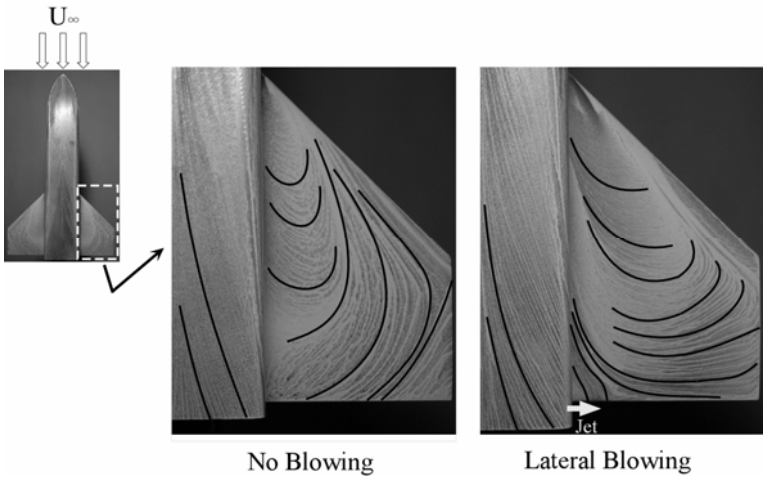

(b) “Square” model

Fig. 11 Oil flow visualization result of “Triangular” and “Square” model at α=25°, C_μ=0.015 and M_∞=0.29 (top view).

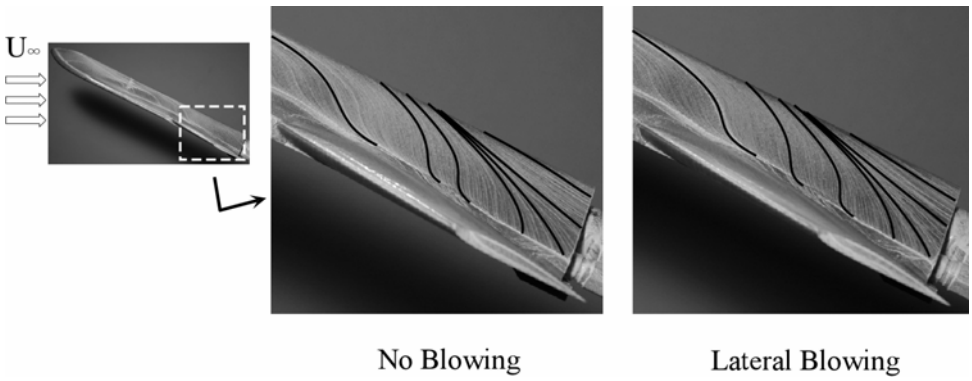

(a) “Triangular” model

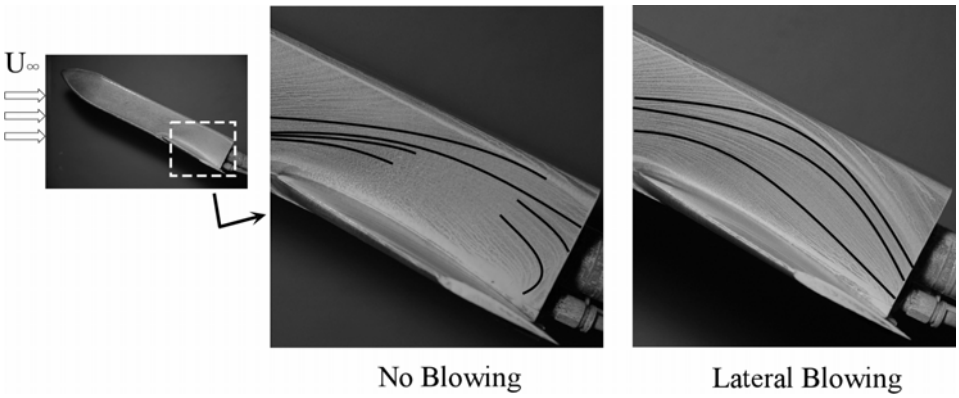

(b) “Square” model

Fig. 12 Oil flow visualization result of “Triangular” and “Square” model at α=25°, C_μ=0.015 and M_∞=0.29 (side view).

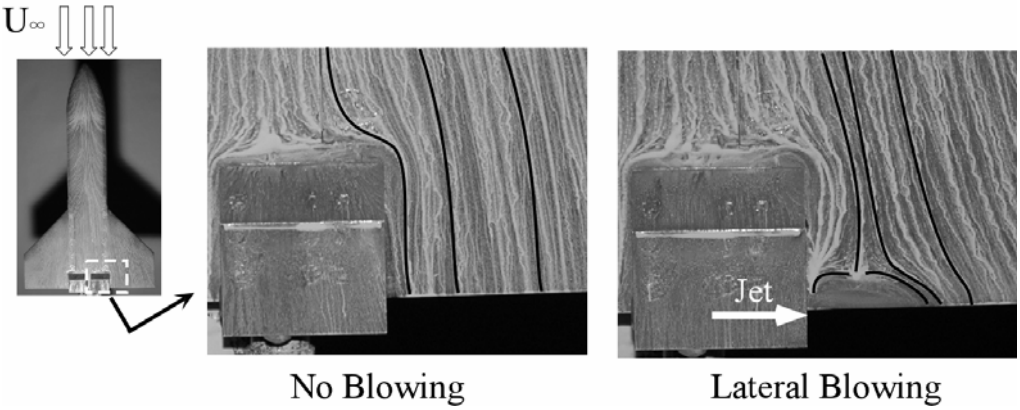

(a) “Triangular” model

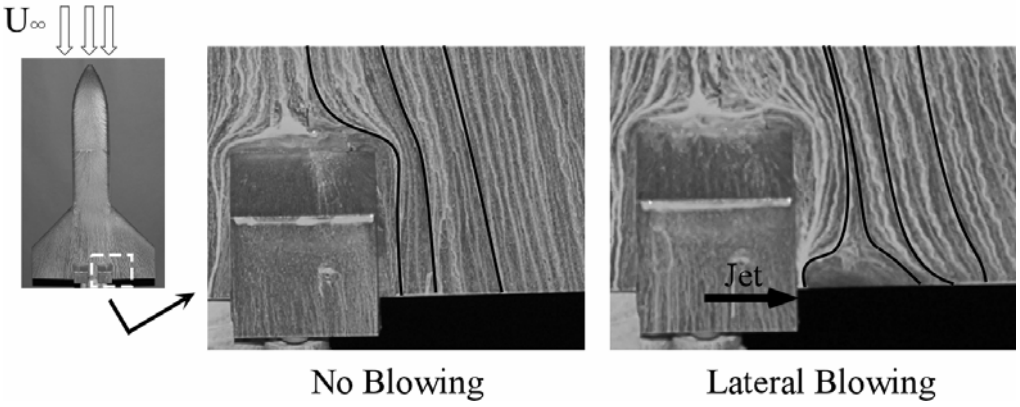

(b) “Square” model

Fig. 13 Oil flow visualization result of “Triangular” and “Square” model at α=25°, C_μ=0.015 and M_∞=0.29 (lower view).

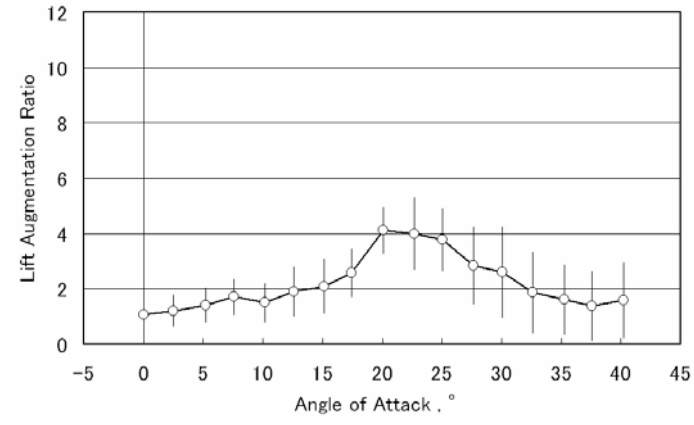

(a) “Triangular” model

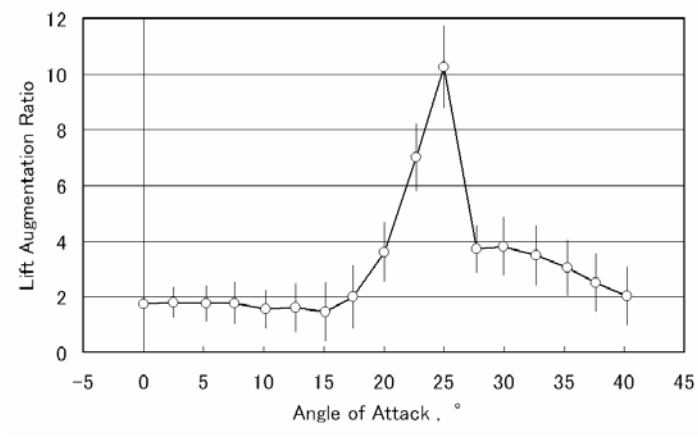

(b) "Square" model

Fig. 14 Blowing efficiency in lift at C_μ=0.015 and M_∞=0.29.

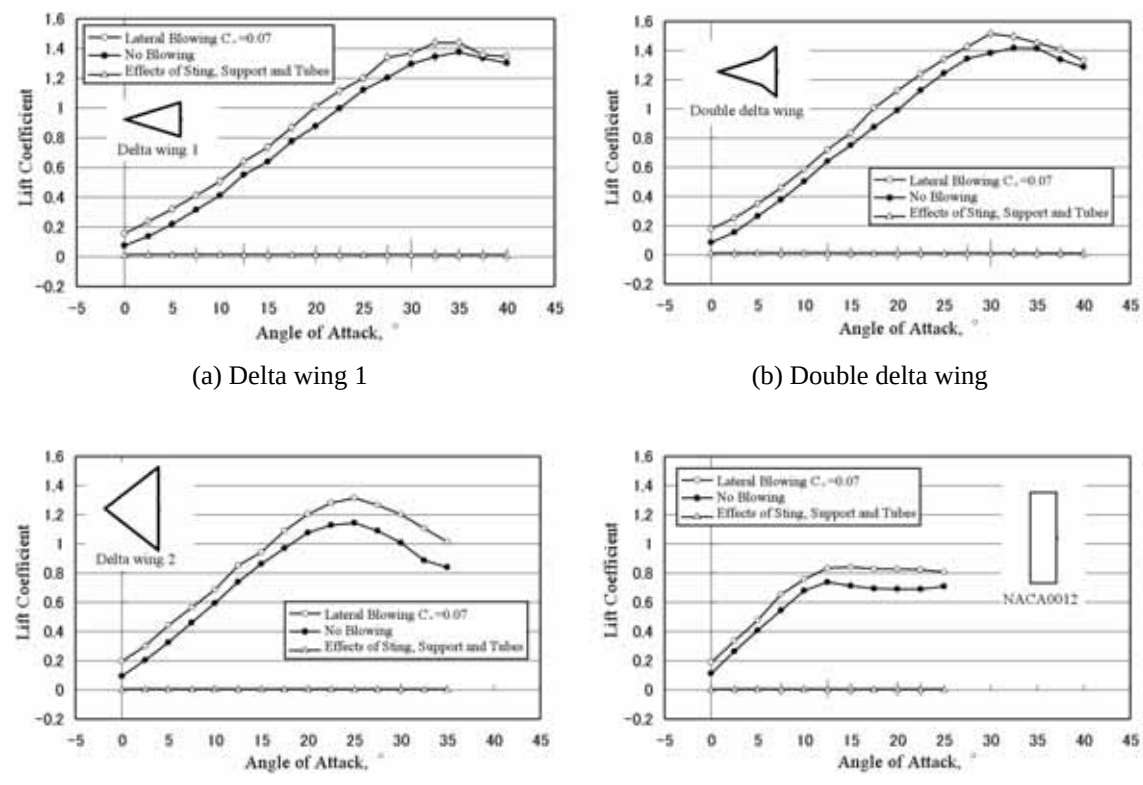

(a) Delta wing 1

(b) Double delta wing

(c) Delta wing 2

(d) NACA0012

Fig. 15 Aerodynamic characteristics of different planform models at U_∞=20 m/s.

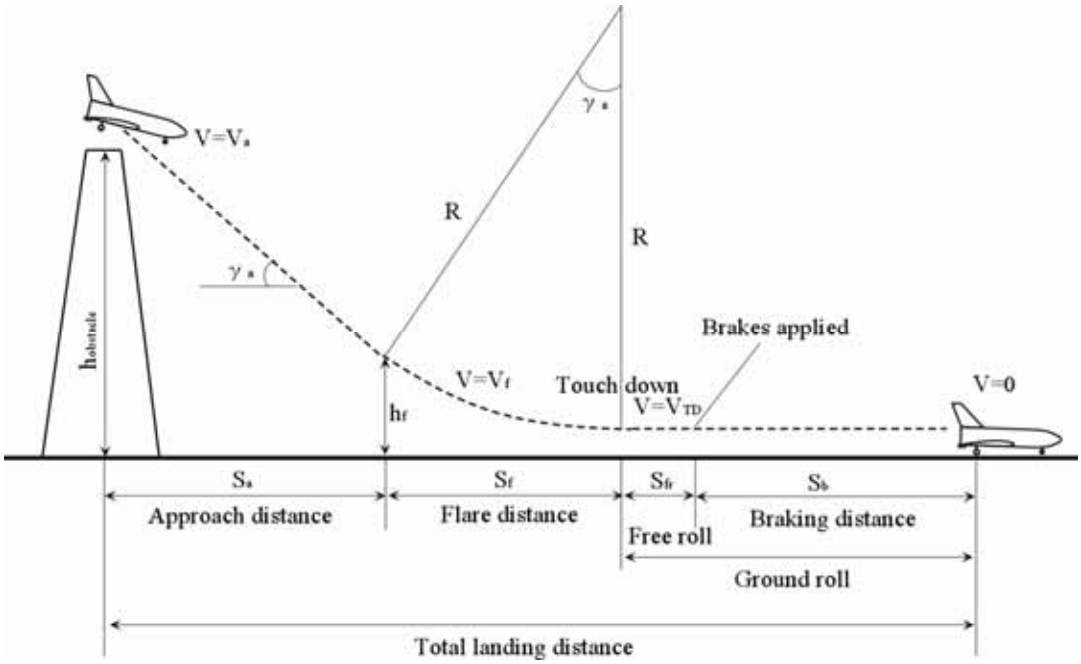

Fig. 16 Landing phase.

Table 3 Conditions for calculation of required air amount.

Length	Landing Weight	Projection Area	Density	C_{Lmax}	Approach Angle
29.6 m	85.3 ton	235.2 m^2	1.225 kg/cm^2	0.83	8 °

Table 4 Calculation results.

Time	Air Amount
9.1 s	1,321 kg